

# Capacitive detection of subband structure in the electron gas in a wide parabolic GaAs/Al<sub>x</sub>Ga<sub>1-x</sub>As quantum well

A. J. Rimberg, Scott Yang, Jed Dempsey, J. H. Baskey, and R. M. Westervelt  
*Division of Applied Sciences and Department of Physics, Harvard University, Cambridge, Massachusetts 02138*

M. Sundaram and A. C. Gossard  
*Materials Department, University of California, Santa Barbara, California 93106*

(Received 12 June 1992; accepted for publication 18 November 1992)

Profiles of the capacitance  $C(V_g)$  between a front gate and the electron gas in a wide parabolic well and its derivative  $dC/dV_g$  are used to study the subband structure and uniformity of the electron gas layer. Subband depopulation events are detected as peaks in the derivative profile  $dC/dV_g$  as the width of the electron gas is reduced by application of the gate voltage  $V_g$ . To separate depopulation events from nonuniformities in electron density, derivative profiles are repeated for increasing in-plane magnetic fields: depopulation peaks move to smaller gate voltages and disappear at characteristic fields, while nonuniformities remain fixed and are accentuated in strong fields.

Wide parabolic quantum wells (WPBWs) have received much attention in the past few years as a system in which an electron gas of variable thickness and subband structure can be studied.<sup>1-5</sup> These wells are also interesting in that they can provide an electron gas with low three dimensional (3D) density ( $\sim 5-25 \times 10^{15} \text{ cm}^{-3}$ ) and good uniformity over wide ( $\sim 2000 \text{ \AA}$ ) regions.<sup>4,5</sup> Recently, Wixforth *et al.*<sup>2</sup> and Sundaram *et al.*<sup>3</sup> have turned to measurements of the capacitance profile  $C(V_g)$  between a front gate and the electron gas in a WPBW as a function of gate voltage  $V_g$  to probe changes in the subband structure of the system as the gas width is changed. Such measurements are difficult for two reasons. First, changes in capacitance associated with changes in subband occupancy can be quite small ( $\sim$  one part in  $10^3$ ) compared to the total capacitance, requiring high sensitivity. Second, a local variation in electron density due to imperfect well shape will give rise to a feature in  $C(V_g)$  similar to a subband depopulation, but potentially much larger.

We report here the detection of peaks in the derivative profile  $dC/dV_g$  for a wide parabolic well which can be unambiguously identified with subband depopulations. An in-plane magnetic field  $H$  is used to separate peaks due to subband depopulations from features due to nonuniformities in the electron gas. The depopulation peaks move to smaller gate voltage with increasing field  $H$ , in excellent agreement with self-consistent calculations; the depopulation fields  $H_d$  at which the peaks are projected to reach zero gate voltage are also in excellent agreement with in-plane magnetoresistance measurements. In the quantum limit for which only one subband is occupied, we obtain an approximate charge density profile<sup>6,7</sup> uniform to  $\pm 20\%$  across the electron gas layer.

The total inverse capacitance<sup>2,8</sup> of the electron gas in an ideal wide parabolic well can be expressed as the sum of geometric and quantum parts:

$$\frac{1}{C} = \frac{1}{C_{\text{geom}}} + \frac{1}{C_q} \quad (1)$$

The geometric capacitance is associated with the classical electron density profile, which we model as a uniform slab at the 3D design density of the well  $n_{3D}$  with sharp edges, giving:

$$C_{\text{geom}} = \epsilon \epsilon_0 A \left( z_0^2 + \frac{2\epsilon \epsilon_0 V_g}{en_{3D}} \right)^{-1/2} \quad (2)$$

Here  $A$  is the area of the gate,  $z_0$  is the distance from the gate to the front of the slab at  $V_g=0 \text{ V}$ ,  $\epsilon=12.8$  is the dielectric constant of GaAs,  $\epsilon_0$  is the electric permittivity of free space and  $-e$  is the electronic charge. The inverse quantum capacitance  $1/C_q$  is defined via Eq. (1) as the difference between a quantum-mechanical self-consistent calculation<sup>9</sup> of the total inverse capacitance of the electron gas and  $1/C_{\text{geom}}$  from Eq. (2). This difference is associated with changes in the Fermi energy  $E_F$  relative to the electrostatic potential of the geometric model:  $C_q = e^2 A \partial n_s / \partial E_F$ . The Fermi energy has two contributions: a kinetic energy term, and the difference between the true self-consistent and the simple geometric potentials.

The sample chosen for study (PB31) was grown via molecular beam epitaxy using the digital alloy technique.<sup>10</sup> It contains a well of nominal width  $2000 \text{ \AA}$  and height  $175 \text{ meV}$ , with nominal electron density  $n_{3D} = 2.5 \times 10^{16} \text{ cm}^{-3}$ . Previous transport measurements in both transverse<sup>5</sup> and in-plane<sup>11</sup> magnetic fields demonstrated that the density and subband energies of the electron gas are in excellent agreement with theory, and that the electron layer is  $900 \text{ \AA}$  wide with three occupied subbands. For the present work, a Cr/Au front gate was added to the sample, which caused only a small (2%) reduction in Hall sheet density to  $n_s = 2.26 \times 10^{11} \text{ cm}^{-2}$ . The sample was cooled in the dark inside a <sup>3</sup>He cryostat; to change sample orientation with respect to the magnetic field, we thermally cycled and remounted it. The capacitance profile  $C(V_g)$  between the gate and the electron gas was measured by applying a variable dc bias  $V_g$  with a superimposed sinusoidal oscillation (20 mV rms at 402 Hz) which induces a small ( $\sim 1.7\%$ ) change in sheet density at  $V_g=0 \text{ V}$ . The ac current was

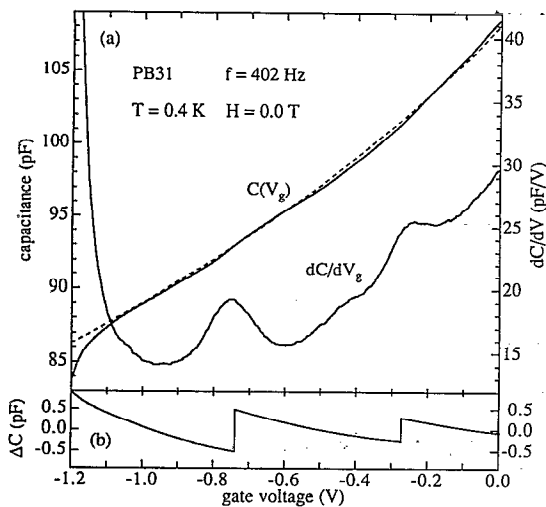


FIG. 1. (a) Capacitance  $C(V_g)$  and derivative  $dC/dV_g$  profiles vs gate voltage  $V_g$  at zero magnetic field. The dashed line is a fit to the geometric capacitance from Eq. (2). (b) Theoretical quantum contribution to the capacitance  $\Delta C \equiv -C_{\text{geom}}^2/C_q$  from self-consistent calculations; steps occur in  $\Delta C$  at subband depopulations.

amplified and detected using standard lock-in techniques. The derivative profile  $dC/dV_g$  was simultaneously measured at twice the fundamental frequency with a second lock-in amplifier. We found no significant change in  $C(V_g)$  or  $dC/dV_g$  for oscillation frequencies and amplitudes in the range 101–1010 Hz and 10–30 mV rms. The measured impedance was purely capacitive except near pinch-off.

A typical measured capacitance profile  $C(V_g)$  is shown in Fig. 1(a) for zero in-plane field  $H$ . As shown  $C(V_g)$  decreases smoothly with  $V_g$  until pinch-off occurs at  $V_g = -1.2$  V. The geometric capacitance  $C_{\text{geom}}$  from Eq. (2), shown as the dotted curve, provides an excellent fit to the measured profile indicating that this simple classical approximation is fairly good. The gate area  $A = 3.4 \times 10^{-3}$  cm<sup>2</sup> determined by the fit is 11% less than the area measured under a microscope. The values of the other parameters  $z_0$  and  $n_{3D}$  in  $C_{\text{geom}}$  were determined by fits to depopulation peak voltages as discussed below. Small differences between the measured profile  $C(V_g)$  and  $C_{\text{geom}}$  are shown clearly as two peaks in the measured derivative profile  $dC/dV_g$  in Fig. 1(a). As demonstrated below, these two peaks are caused by subband depopulations rather than nonuniformities in the electron density profile.

To compare with theory, the change  $\Delta C \equiv C - C_{\text{geom}} \approx -C_{\text{geom}}^2/C_q$  from Eq. (1) due to the quantum capacitance  $C_q$  was determined from self-consistent calculations<sup>9</sup> for the ideal case of zero temperature and no disorder. As shown in the plot of  $\Delta C$  in Fig. 1(b), each depopulation event causes a vertical step in  $\Delta C$  due to a change in slope of the Fermi energy versus sheet density. Each step in  $\Delta C$  corresponds to a delta function peak in the derivative profile  $dC/dV_g$ ; for experimental data these peaks are broadened by disorder and temperature. The profile  $\Delta C$  shown in Fig. 1(b) is a fit obtained by varying the parameters  $n_{3D}$  and  $z_0$  to match the voltages of the two steps in  $\Delta C$  with the two peaks in the measured derivative profile  $dC/dV_g$ .

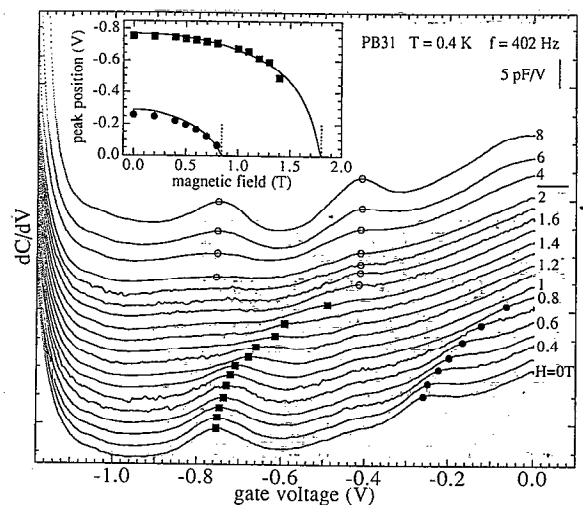


FIG. 2. Derivative profiles  $dC/dV_g$  vs gate voltage  $V_g$  offset for a series of in-plane magnetic fields  $H=0-8$  T. From 0 to 2 T the field increment is  $\Delta H=0.1$  or 0.2 T; from  $H=2$  to 8 T,  $\Delta H=2$  T. Gate voltages associated with depopulation events (solid squares and circles) and nonuniformities (open circles) are indicated. The inset shows the field dependence of the measured gate voltages for depopulation events (solid squares and circles), together with theoretical calculations (solid lines). Depopulation fields at zero gate voltage obtained from magnetotransport measurements are also indicated (vertical dashed lines).

The best fit is for  $n_{3D} = 2.4 \times 10^{16}$  cm<sup>-3</sup> and  $z_0 = 3600$  Å, 4% smaller and 16% larger than their nominal values assuming symmetric filling of the parabolic well above the center. Furthermore, the areas of the peaks in  $dC/dV_g$  are in good agreement with the theory: the measured areas 0.63 and 0.30 pF for the peaks at  $-0.75$  and  $-0.26$  V are slightly smaller than the corresponding theoretical step sizes in  $\Delta C = 1.0$  and 0.54 pF. Thus a fit by three parameters  $n_{3D}$ ,  $z_0$ , and  $A$  gives excellent agreement with theory for both the geometric and quantum parts of the calculated capacitance, including the strength of depopulation peaks.

To separate subband depopulation peaks from features due to nonuniformities, a series of derivative profiles  $dC/dV_g$  were recorded for increasing magnetic fields  $H$  applied in the plane of the parabolic well, as shown in Fig. 2. In this geometry, the subbands of the well potential couple with Landau levels, and higher subbands depopulate at characteristic magnetic fields  $H_d$  for zero gate voltage. Similarly, one expects the gate voltage  $V_g$  at which higher subbands depopulate to decrease with  $H$ , and depopulation peaks in  $dC/dV_g$  to move to less negative voltage  $V_g$  as  $H$  increases, reaching zero gate voltage at  $H_d$ . This behavior is, in fact, observed for the depopulation peaks in Fig. 2, labeled as solid squares and solid circles, which move to less negative gate voltage and disappear for moderate field  $H < 2$  T. The peak positions are plotted versus magnetic field  $H$  in the inset to Fig. 2, and are in excellent agreement with a self-consistent Hartree calculation<sup>12</sup> of the field-dependent depopulation voltages, shown as the solid lines, performed with no new adjustable parameters. The only inputs to theory are  $n_{3D}$  and  $z_0$  from the fit above at  $H=0$  T, and the measured Hall sheet density  $n_s$ . In-plane mag-

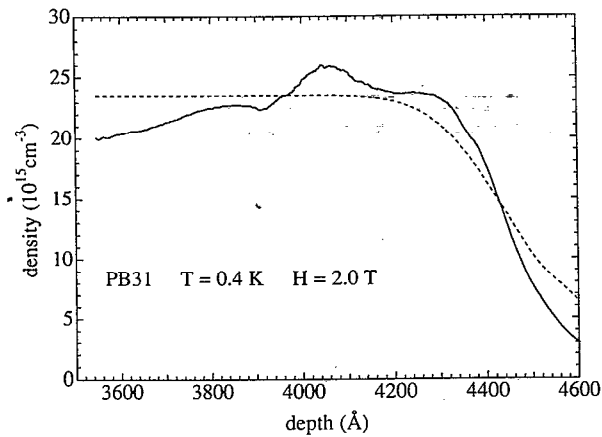


FIG. 3. Classical charge density profile  $n(z)$  (solid line) and smeared rectangular profile (dashed line) modeling quantum uncertainty in the electron position.

netotransport measurements<sup>11</sup> give independent measurements of the depopulation fields  $H_d \approx 0.8$  and 1.8 T at zero gate voltage for the third and second subbands of this sample, shown in the inset to Fig. 2 as vertical dashed lines, which are in excellent agreement with theory. The detailed quantitative agreement between capacitance profiles, theory, and magnetotransport measurements allows us to unambiguously identify the peaks in the derivative profile that are due to subband depopulation.

In contrast to depopulation events, features due to nonuniformities in the electron density profile remain at fixed gate voltage, and grow stronger with increasing in-plane fields  $H$ , due to electron localization as the magnetic length  $\ell_H = (\hbar/eH)^{1/2}$  is reduced. Features of this type are found in the derivative profiles shown in Fig. 2 for stronger in-plane fields  $H > 2$  T, and are labeled by open circles. The classical electron density profile  $n(z)$  obtained from  $C$  and  $dC/dV_g$  using the geometrical model<sup>13</sup> is shown in Fig. 3 as the solid line for the magnetic quantum limit ( $H = 2.0$  T) for which only the lowest subband is occupied. As shown, variations in  $n(z)$  are small, indicating a high degree of uniformity in the electron gas for moderate in-plane magnetic fields. The density profile  $n(z)$  in Fig. 3 is smeared by quantum effects, modeled by the dotted curve in Fig. 3, which is a rectangular profile convolved with a Gaussian of variance  $\ell_H^2/2$ . The sheet density  $n_s = \int n(z) dz$  is conserved<sup>7</sup> in a quantum treatment and the integral  $\int n(z) dz$

of the density profile  $n(z)$  in Fig. 3 agrees with the measured Hall sheet density to within  $\sim 6\%$ .

In conclusion, we have detected peaks in the derivative profile  $dC/dV_g$  for the gate-to-gas capacitance in a wide parabolic well which can be unambiguously identified with subband depopulations. At zero magnetic field, a quantitative fit to theory is obtained for both the capacitance and derivative profiles which give parameter values in agreement with nominal values. An in-plane magnetic field is applied to separate depopulation peaks from features due to nonuniformities. The field dependence of the depopulation peaks is in excellent agreement with theoretical calculations using no new adjustable parameters, as well as with in-plane magnetotransport measurements. For moderate magnetic fields in the quantum limit the electron density profile  $n(z)$  is found to be uniform to  $\pm 20\%$ .

We thank P. F. Hopkins for helpful comments. One of us (J.H.B.) acknowledges support from the Natural Sciences and Engineering Research Council of Canada. This work was supported at Harvard by NSF Grants DMR-91-19386 and DMR-89-20490 and at Santa Barbara by AFOSR Grant AFOSR-91-0214.

<sup>1</sup>E. G. Gwinn, R. M. Westervelt, P. F. Hopkins, A. J. Rimberg, M. Sundaram, and A. C. Gossard, *Phys. Rev. B* **39**, 6260 (1989); T. Sajoto, J. Jo, M. Santos, and M. Shayegan, *Appl. Phys. Lett.* **55**, 1430 (1989).

<sup>2</sup>A. Wixforth, M. Sundaram, K. Ensslin, J. H. English, and A. C. Gossard, *Appl. Phys. Lett.* **56**, 454 (1990).

<sup>3</sup>M. Sundaram, K. Ensslin, A. Wixforth, and A. C. Gossard, *Superlatt. Microstruct.* **10**, 157 (1991).

<sup>4</sup>E. G. Gwinn, P. F. Hopkins, A. J. Rimberg, R. M. Westervelt, M. Sundaram, and A. C. Gossard, *Phys. Rev. B* **41**, 10700 (1990).

<sup>5</sup>P. F. Hopkins, A. J. Rimberg, E. G. Gwinn, R. M. Westervelt, M. Sundaram, and A. C. Gossard, *Appl. Phys. Lett.* **57**, 2823 (1990).

<sup>6</sup>D. P. Kennedy, P. C. Murley, and W. Kleinfelder, *IBM J. Res. Dev.* **12**, 399 (1968).

<sup>7</sup>H. Kroemer, W. Y. Chien, J. S. Harris, Jr., and D. D. Edwall, *Appl. Phys. Lett.* **36**, 295 (1980).

<sup>8</sup>T. P. Smith, B. B. Goldberg, P. J. Stiles, and M. Heiblum, *Phys. Rev. B* **32**, 2696 (1985).

<sup>9</sup>A. J. Rimberg and R. M. Westervelt, *Phys. Rev. B* **40**, 3970 (1989).

<sup>10</sup>M. Sundaram, A. C. Gossard, J. H. English, and R. M. Westervelt, *Superlatt. Microstruct.* **4**, 683 (1988).

<sup>11</sup>R. M. Westervelt, A. J. Rimberg, P. F. Hopkins, E. G. Gwinn, M. Sundaram, and A. C. Gossard, in *Proceedings of the 20th International Conference on the Physics of Semiconductors*, Thessaloniki, 1990, edited by E. Anastassakis and J. D. Joannopoulos (World Scientific, Singapore, 1990), Vol. 2, p. 1085.

<sup>12</sup>J. Dempsey (unpublished); see also M. P. Stopa and S. Das Sarma, *Phys. Rev. B* **40**, 10048 (1989), and L. Brey and B. I. Halperin, *Phys. Rev. B* **40**, 11634 (1989).

<sup>13</sup>See, for example, D. C. Look, *Electrical Characterization of GaAs Materials and Devices* (John Wiley, Chichester, 1989).